Systematic analysis of diffuse rear reflectors for enhanced light trapping in silicon solar cells

Florian Pfeffer ^{1,2}, Johannes Eisenlohr *¹, Angelika Basch ^{1,2}, Benjamin G. Lee ^{1,3}, Martin Hermle ¹, Jan Christoph Goldschmidt ¹

¹Fraunhofer Institute for Solar Energy Systems (ISE), Heidenhofstrasse 2, 79110 Freiburg, Germany

²University of Applied Sciences, Eco-Energy Engineering, Stelzhamerstraße 23, 4600 Wels, Austria

³National Renewable Energy Lab, 15013 Denver West Parkway, Golden CO 80401 USA

*Corresponding author, e-mail address: Johannes.Eisenlohr@ise.fraunhofer.de,

telephone: +49 (0) 761/4588-5562

Abstract

Simple diffuse rear reflectors can enhance the light path length of weakly absorbed near infrared light in silicon solar cells and set a benchmark for more complex and expensive light trapping structures like dielectric gratings or plasmonic particles. We analyzed such simple diffuse rear reflectors systematically by optical and electrical measurements. We applied white paint, TiO₂ nanoparticles, white backsheets and a silver mirror to bifacial silicon solar cells and measured the enhancement of the external quantum efficiency for three different solar cell geometries: planar front and rear side, textured front and planar rear side, and textured front and rear side. We showed that an airgap between the solar cell and the reflector decreases the absorption enhancement significantly, thus white paint and TiO₂ nanoparticles directly applied to the rear cell surface lead to the highest short circuit current density enhancements. The short circuit current density gains for a 200 µm thick planar solar cell reached up to 1.8 mA/cm², compared to a non-reflecting black rear side and up to 0.8 mA/cm² compared to a high-quality silver mirror rear side. For solar cells with textured front side the short circuit current density gains are in the range between 0.5 and 1.0 mA/cm² compared to a non-reflecting black rear side and do not significantly depend on the angular characteristic of the rear side reflector but mainly on its absolute reflectance.

Keywords

light trapping, diffuse rear reflectors, silicon solar cell, bifacial solar cell

1. Introduction

Light trapping in silicon solar cells is a key aspect for future efficiency increases and cost reductions. Due to the weak absorption of photons in the near infrared (NIR) between 900 and 1200 nm in crystalline silicon, structures that enhance the light path length have to be applied. At the front surface such a light path length enhancement can be reached by pyramidal front side textures, which also cause a significant reduction of reflection losses over the complete spectrum [1–4]. Light trapping can also be improved at the rear surface. Goetzberger [5] and Yablonovitch [6] described the improvement of a solar cell using a Lambertian rear reflector. Following this pioneering work, many devices have been realized using rather simple fabrication techniques. For example, Cotter et al. [7] investigated the optical intensity of light in layers of silicon with diffuse rear reflectors and deduced, that the refractive index of the diffuse reflector should be as high as possible. Berger et al. [8] investigated commercial white paint as a diffuse rear reflector. Applied to 1-2 μm thin-film polycrystalline silicon solar cells, they measured a short circuit current density

gain of up to 2.87 mA/cm², which led to an overall J_{SC} of 9.91 mA/cm². Barugkin et al. [9] used Ag nanoparticles covered with a BaSO₄ based white paint as a rear reflector. They used a 260 µm thick solar cell with a reactive ion etched textured front side. They reached a J_{SC} of 5.7 mA/cm² between 990 and 1200 nm corresponding to a J_{SC} gain of 2.3 mA/cm² compared to solar cells with planar front and rear. Binders used in usual white paints are organic materials with a low refractive index (1.4-1.7), which absorb light [10] in the near infrared. Therefore, a binder-free, fully covered rough rear surface with a high refractive index is advantageous. Lee et al. [11] dispersed TiO₂ nanoparticles in deionized water with a pH value of 10 and deposited them via drop coating. With this method it is possible to cover the rear side with TiO₂ nanoparticles only. However, the alkalized suspension can harm the rear side of the solar cell. The TiO_2 nanoparticles were placed behind 2.5 μm thick crystalline silicon solar cells. They presented a ΔJ_{SC} of 3.91 mA/cm², which leads to an overall J_{SC} of 13.46 mA/cm². In comparison, Basch et al. [10] dispersed the TiO₂ nanoparticles in pH neutral water, which does no harm the solar cells. Additionally, the TiO₂ nanoparticles were compared with white paint and show an enhanced reflectivity [10]. The TiO2 nanoparticles were placed behind 2 µm thick amorphous silicon cells. They presented a ΔJ_{SC} of 4.8 mA/cm², which leads to an overall J_{SC} of 18.7 mA/cm². Ingenito et al. applied TiO₂ based white paint as rear reflectors for 180 µm thick, both side textured crystalline silicon solar cells and demonstrated a current density gain of 0.6 mA/cm² compared to no rear reflector [12]. For the deposition of TiO₂ particle layers also on large scale, methods are presented in literature using simple and scalable processes [13]. In [14] Frank et al. simulated the potential photocurrent density $J_{\rm ph}$ based on the measured properties of different diffuse rear reflectors for 200 µm thick silicon wafers with three different combinations of surface morphologies: planar front and rear surface (pp), textured front (random pyramids) and planar rear surface (tp), or both sides textured with random pyramids (tt). They compared white paint, polytetrafluoroethylene (PTFE), white paper and a silver mirror. One conclusion of the work of Frank et al. was the prediction that both-side textured solar cells with a good rear side reflector show the overall highest photo current density.

Furthermore, a large variety of more complex light trapping structures is reported in literature, including periodic gratings [15–21], metal structures utilizing plasmonic effects [22,23] or combinations of nanotextures and dielectric rear reflectors [24]. Bermel et al. showed that the absorption in thin film silicon solar cells can be enhanced by a relative amount of over 30% using photonic crystals [16]. Peters et al. [18] simulated a short circuit current density (J_{SC}) enhancement of 1.85 mA/cm² for a 40 μ m thick silicon solar cell due to a diffractive grating on the rear side compared to a specular rear side. This leads to an overall efficiency increase of 1% and a total efficiency of 18.7%. Mellor et al. [25] predicted a J_{SC} enhancement of up to 1.5 mA/cm² for a 200 μ m thick silicon solar cell with nanoimprinted diffraction gratings at the rear leading to an overall J_{SC} of 38 mA/cm². Tucher et al. [26] presented short circuit current density gains due to a diffractive rear side grating of up to 1.2 mA/cm² in 250 μ m thick silicon solar cells with planar front side compared to a mirror on the rear side. Eisenlohr et al. [21] demonstrated a J_{SC} enhancement of 1.4 mA/cm² due to a sphere grating rear side (also compared to a mirror at the rear side) for 200 μ m thick solar cells with planar front side.

Many of the experimental studies introduced above investigated one specific rear side reflector on one specific solar cell type and geometry. Hence it is difficult to compare the presented results quantitatively. Therefore, in this paper we present a systematic analysis of simple diffuse rear reflectors. We investigated different white backsheets, white paints and TiO₂ nanoparticles. For reference we also investigated a silver mirror and black cardboard as rear reflectors. Furthermore, we considered different surface geometries. Samples with planar front and rear were analyzed, because

any light trapping effects caused by a diffuse rear reflector are most pronounced in such a structure. Samples with textured front and planar rear were included, as this configuration is widely used for high efficiency silicon solar cells [27]. Finally, both sides textured samples were considered, because the simulations of Frank et al. [14] suggested the highest current potential for these structures. Figure 1 shows the principle structure of the measured systems with a diffuse rear reflector. We placed the white paint and TiO₂ nanoparticles directly on the rear side – no air gap remained. On the other hand we placed the backsheets and the mirror behind the rear side with a remaining air gap. The difference between the two setups is that in a) the light can be scattered into a broader angular range within the silicon while in b) due to refraction, scattered light is confined to a cone with an opening angle of about 16° within the silicon

We analyzed the different direct and diffuse reflectivities of the used materials and measured the reflectance and transmittance of silicon wafers with all different reflectors to estimate the possible absorption enhancement. Finally, we tested the best rear reflectors on the device level. For this purpose we used bifacial solar cells originally optimized for experiments with upconverting materials at the rear side [28] and measured the external quantum efficiency (EQE) and the IV-curve for the different rear reflectors.

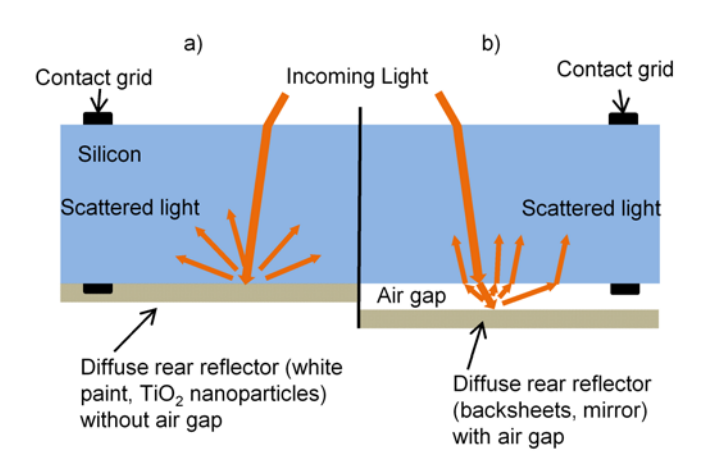


Figure 1: Schematic structure of the measured system. It is possible to place the diffuse rear reflector behind the solar cell without (a) and with (b) an air gap.

2. Materials and Methods

For the optical and electrical measurements we placed different reflectors as summarized in Table 1 behind wafers and solar cells, respectively. Their reflectance measured in air is displayed in Figure 2.

Table 1: Used rear reflectors.

Air + Mirror:	A silver mirror (Company: Thorlabs, reflectivity over 95% between 600 and 1400 nm) was placed behind the wafer while a gap of air remains between the wafer and the mirror.
Air + Black Cardboard:	Black cardboard (reflectivity lower than 3%, transmission lower than 0.4% between 600 and 1400 nm) was placed behind the wafer while a gap of air remains between the wafer and the black cardboard.
Air + Backsheet:	Three different white backsheets (Company: Isovoltaic, Material: 3554 and 2442w; Company: Dunmore, Material: PPE+) were located behind the wafer while an air gap remains between the wafer and the backsheets.

White Paint:	White paint was placed directly on the rear side of the wafer. (Company: OBI, Material: Premium white color; Company: Schöner Wohnen, Material: Polar white color; Company: Schmincke, Material: Acryl color, titanium white)
TiO ₂ Nanoparticles:	TiO ₂ nanoparticles with an average size of 1.106 μm were placed directly on the rear side of the solar cell precursors. Particles and method are described in Basch et al. [10]. (Company: Treibacher Industrie AG, Material: TiO ₂ -100, L32090)

For dense, pin-hole free coverage, we applied three layers of white paint on the wafer with a bristle brush. The single layers were dried for 2 hours at room temperature. For the TiO₂ coating we used a combination of the methods established by Basch et al. [10] and Lee et al. [11]. 10 g rutile TiO₂ nanoparticles were dispersed in 100 g purified water and the resulting suspension sonicated for 30 min. The silicon wafers were put onto a hot plate at a temperature of 60 °C where several drops of the suspension were applied onto the wafer for a fully covered rear surface. We repeated the coating process 5 times, with several minutes of drying in between.

For the **optical experiments**, we used 200 μ m thick, shiny-etched, 0.8-1.2 Ω cm, (100)-oriented *n*-type float zone (FZ) silicon wafers, with three different combinations of surface morphologies: planar front and rear surface (pp), textured front surface with random pyramids and planar rear surface (tp), or both sides textured with random pyramids (tt). To calculate the absorptance A=I-R-T, the reflectance R and transmittance T were measured by using a spectrophotometer with an integrating sphere (Varian Cary 5000). The illuminated area for all optical measurements was approximately 10 mm by 5 mm. The angle dependent measurements of the diffuse rear reflectors were conducted with a Fourier-spectrometer.

For the **electrical experiments,** we used bifacial solar cells fabricated at Fraunhofer ISE with three different combinations of surface morphologies [28]: planar front and rear surface (pp), textured front surface with inverted pyramids and planar rear surface (tp), or both sides textured with inverted pyramids (tt). Besides the surface morphology, the three solar cell types were processed similarly. As base material, 4 inch float zone n-type silicon wafers with a resistivity of 1 Ω cm and a thickness of 200 μ m were used. On each wafer seven cells with an active area of 2x2 cm² were fabricated. A 10 nm thick Al₂O₃ electrical passivation layer was deposited on both sides by atomic layer deposition. The used solar cells have been originally designed for experiments with upconverting materials at the rear side and hence e.g. antireflection coating thicknesses are not optimized for a standard use. The pp and tp bifacial solar cells have a full back surface field (BSF) and a 120 nm thick SiN_x antireflection coating (ARC) on the rear side. The front side consists of a double layer ARC made of 85 nm SiN_x and 105 nm MgF₂. The tt bifacial solar cells have a local BSF underneath the metal contacts and a 120 nm thick SiN_x ARC on the rear side. The front side features a double layer ARC made of 110 nm SiN_x and 100 nm MgF₂. The front and rear side metallization grid are aligned, but feature different finger thicknesses.

For all measurements, we mounted the bifacial solar cells in a copper frame that is electrically connected to the busbar of the rear side of the cell and hence works as rear contact.

Additionally, for light beam induced current (LBIC) measurements, we used a bifacial solar cell with an active area of 12.5x12.5 cm². For this cell we used a both side textured 6 inch FZ n-type silicon wafer as base material with a resistivity of 0.8-1.2 Ω cm and a thickness of 250 μ m.

The external quantum efficiency (EQE) and the LBIC was measured with the solar cell analysis system LOANA (pv tools) and the IV-measurements were done with an AM 1.5g STC [29] solar simulator (Oriel, class B). For all electrical measurements the full cell area was illuminated.

3. Results and Discussion

3.1. Reflection of used materials

To compare the different rear reflectors, we measured the hemispheric reflectance using an integrating sphere; results are shown in Figure 2. Overall the TiO₂ nanoparticles and the mirror show the highest reflectance, but while the mirror reflects all light specularly, the nanoparticles show strong scattering. Acryl color and the backsheet 3554 showed the highest reflectance of the white paints and of the different backsheets, respectively. Accordingly these materials, denoted in the following as backsheet, white paint and TiO₂ nanoparticles, were chosen for further analysis.

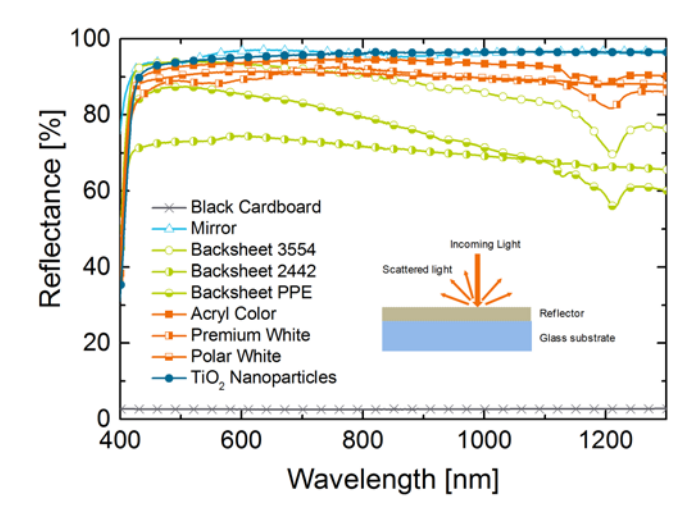


Figure 2: Measured reflectance of the different rear reflectors.

To compare the different scattering distributions of the diffuse rear reflectors, we conducted an angle dependent reflectance measurement in air. In addition, scanning electron microscopy (SEM) imaging was done. Figure 3 shows the SEM image of a) the backsheet, b) the white paint and c) the TiO₂ nanoparticles. The white paint also contains TiO₂ particles, but it can be observed that they are dispersed in a binder. The TiO₂ nanoparticles in c) were deposited without an additional binder. Figure 3 d) shows the angularly resolved reflectance of the three reflectors for normal incidence at a wavelength of 1000 nm. The reflectance curve of a perfect Lambertian scatterer is plotted as well. In order to be able to compare the reflectance distribution to the Lambertian scatterer the total reflectance is normalized to the total reflectance of the Lambertian scatterer, which corresponds to an equal area under the curves in Figure 3 d). Figure 2 e) shows the difference compared with the Lambertian scatterer. All three diffuse rear reflectors scatter light similarly to the ideal Lambertian scatterer. For all investigated samples, especially in the case of the backsheet, the forward scattering is slightly higher while the scattering into large angles is slightly lower than in the Lambertian case. Nevertheless, all three reflectors can be regarded as good diffuse reflectors in air.

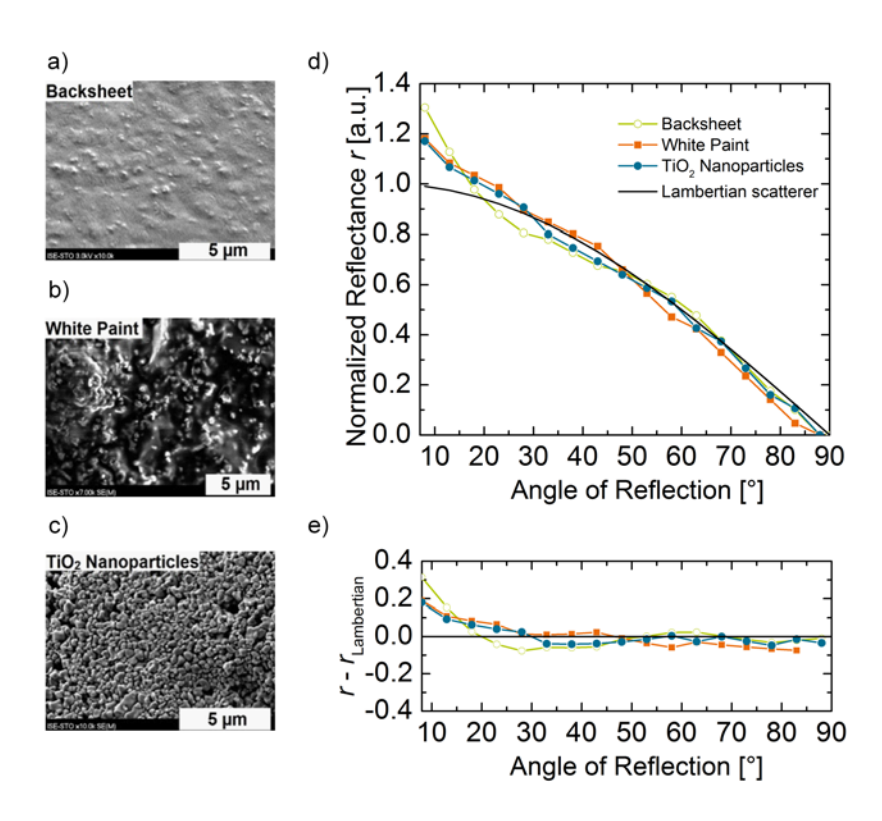


Figure 3: a,b,c) SEM image of the backsheet, white paint and TiO_2 nanoparticles. d,e) Angle-resolved reflectance measurement of the three different diffuse rear reflectors for normally incident light. All curves are normalized to the same total (integrated) reflectance.

3.2. Absorption Enhancement

To determine the absorptance (1-R-T) in the silicon, we measured the reflectance R and the transmittance T of the wafer with and without rear reflector, using an integrating sphere.

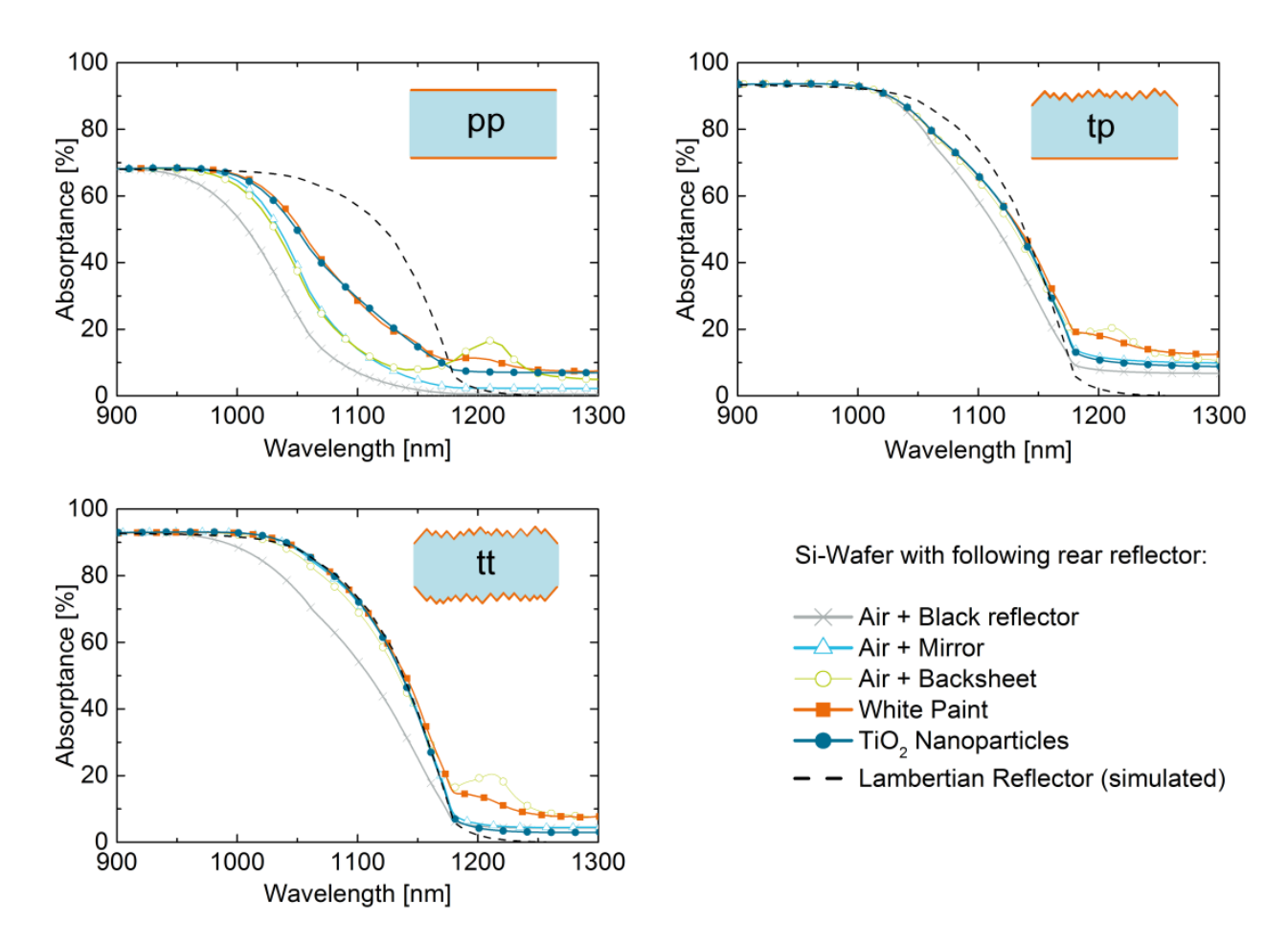


Figure 4: Absorptance (1-*R-T*) of a 200 μm thick silicon wafer with and without a diffuse rear reflector for three different surface morphologies. For comparison, the black dashed line shows the Yablonovitch-Limit related to a Lambertian rear reflector calculated according to [6], with an assumed front side reflectivity set on a fixed value taken from measurement. For the pp-system the highest absorptance is achieved with white paint and TiO₂ nanoparticles, respectively. The absorptance of the systems with air + backsheet and air + mirror is lower. For both tp- and tt-systems the difference between the different rear side reflectors is very small. Only a small absorptance enhancement in comparison to the case without rear reflector can be achieved for the tp textured wafers, while on the tt samples with reflectors the Yablonovitch limit is reached.

In Figure 4 the absorptance of the wafer without any additional rear reflector serves as a lower limit and the Yablonovitch-Limit serves as an upper limit. The Yablonovitch-Limit corresponding to a Lambertian light distribution within the silicon was calculated according to [6], with the front side reflectivity set on the reflectance of the corresponding wafer at a wavelength of 900 nm. As further reference a highly reflective mirror was placed behind the wafer. The absorptance data presented in Figure 4 can be related to the maximal achievable photo current density J_{ph} by

$$J_{ph} = e * \int_{280}^{1200} N_{AM \ 1.5g}(\lambda) * A(\lambda) * d\lambda, \tag{1}$$

where e is the electrical charge of an electron, $N_{AM~1.5g}$ is the photon flux density of the AM 1.5g spectrum and $A(\lambda)$ is the absorptance. The optical test samples featured no ARC layer. With an ARC, because of the higher transmission through the front surface overall more photons reach the rear side of the wafer, which enhances also the absolute value of the photocurrent density gain due to a rear reflector. Therefore, we estimated the photocurrent density that would have been reached with an ARC considering the higher transmission through the front surface. The measured absorptance was multiplied with a correction factor of $(1-r_{ARC})/(1-r_{noARC})$. r_{noARC} is the surface reflectivity without antireflection coating and r_{ARC} the surface reflectivity with the additionally considered antireflection coating. For the

pp wafers a wavelength-dependent correction factor was calculated considering a SiNx/MgF₂ double layer antireflection coating that has also been used for the solar cells in section 3.3. For the tp and tt wafers the correction factor only weakly depends on the wavelength and therefore the actual reflectivity values (at 900 nm) of the solar cells used in section 3.3. have been used. Please note, that the thicknesses of the antireflection coatings are not optimized for highest cell efficiencies due to the original purpose they had been designed for [26]. The modified absorptance was then used in equation (1) to calculate the photo current density. In Figure 5, the calculated J_{ph} for the different surface morphologies with and without ARC is shown.

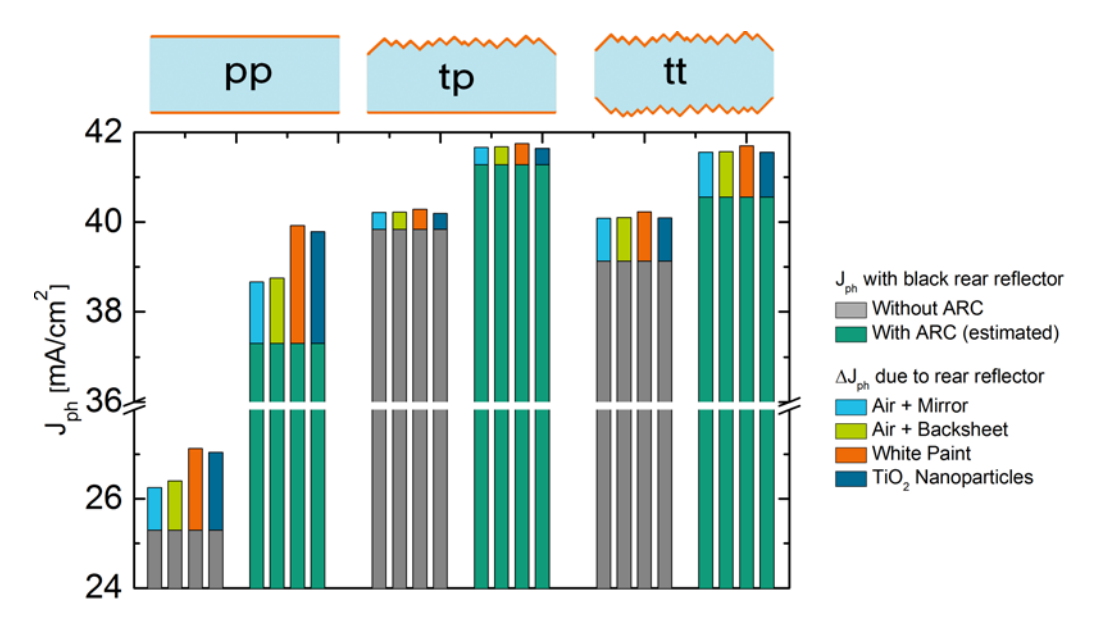


Figure 5: The gray bars show the integrated J_{ph} between 280 and 1200 nm for a black rear reflector and the colored bars the photo current density gain ΔJ_{ph} due to a rear reflector. Additionally the effect of a double layer ARC was estimated, as displayed by the dark green bars.

Especially for the pp system, white paint and TiO_2 nanoparticles show the highest J_{ph} enhancement. This can be explained by the redistribution of light into larger angles within the silicon than for the other investigated structures. A slightly higher gain is predicted for the white paint compared to TiO₂ nanoparticles. This might be caused by the parasitic absorption of the binder contained in the white paint that also contributes to the absorptance, which would not lead to current generation in the solar cell, but cannot be excluded in the type of optical measurements used. The tp-system benefits from all rear reflectors similarly and only by a small amount, no matter whether the rear reflector reflects diffusely or directly. The tt wafers suffer from higher transmission without any rear reflector compared to tp wafers [14], hence a higher $J_{\rm ph}$ enhancement compared to the tp wafers can be observed. However, the gain for the tt wafers is also roughly equal for all kinds of reflectors. This is due to the fact that for tp and tt wafers the system can benefit from additional reflection at the rear side, but not much from additional redistribution of light into different angles, which is already done at the textured surface(s). For wavelengths higher than 1150 nm the measured absorption can be even higher than the calculated Yablonovitch-Limit, which can be caused by parasitic effects and light that is not coupled into the integrating sphere. Note that this does not indicate beyond-Lambertian light trapping. In order to distinguish parasitic absorption effects (as can be seen for example in the case of the backsheet at 1140 nm in Figure 4) and useful absorption in the silicon bulk, leading to a higher J_{SC} , we present electrical measurements of solar cells with these rear reflectors in the following.

3.3. Solar Cell Results

When applying the different rear side reflectors to bifacial solar cells, we measured the IV-curve after the application of each rear side reflector. We did not observe any significant change in the open circuit voltage or the fill factor for any solar cell, which proves that the basic functioning of the solar cells is not affected by the application of the rear side reflectors. To reveal the light trapping effect of the rear reflectors, we conducted detailed EQE measurements for the three solar cell types: pp, tp and tt. Again, black cardboard and a mirror served as reference systems. Additionally, we calculated the Yablonovitch-limit for each solar cell type according to [6], with the front side reflectivity set on the reflectance at a wavelength of 900 nm for the corresponding solar cell.

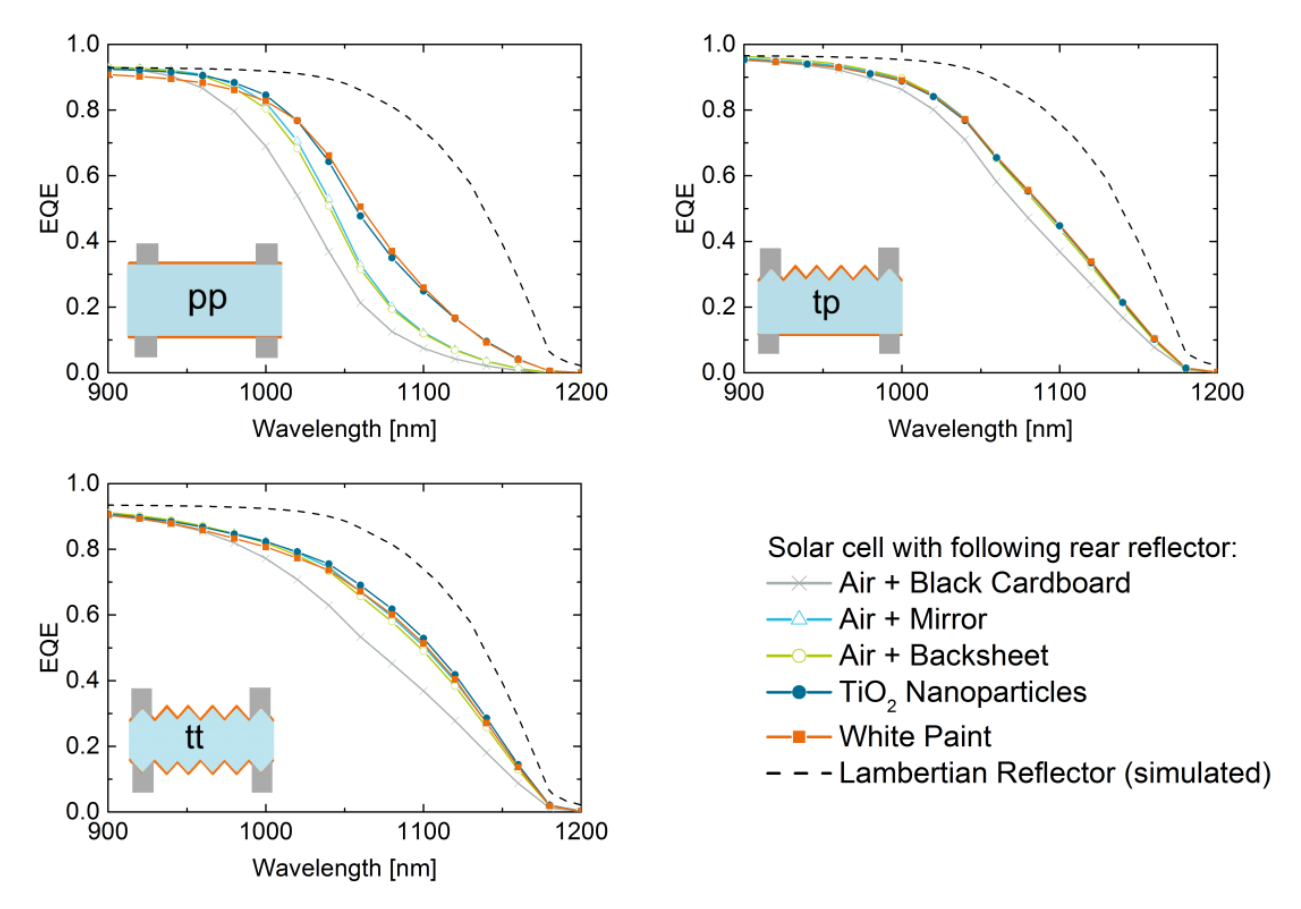


Figure 6: Results of the EQE measurements with the different rear reflectors for solar cells with different surface morphologies. For the pp-solar cells, white paint and TiO₂ nanoparticles show a significantly higher absorption enhancement compared to the backsheet and the mirror. For the tp-solar cells, all rear reflectors show a similar absorption enhancement, while the tt-solar cells benefit slightly more from white paint and TiO₂ nanoparticles as compared to the backsheet and the mirror.

In Figure 6 the EQE of solar cells with the different diffuse rear reflectors is shown. These results are in good accordance with the optical results. The pp-solar cell benefits significantly from a diffuse rear reflector, in particular white paint and TiO₂ nanoparticles lead to a significantly higher EQE enhancement compared to the other materials. The tp-solar cell already has good light trapping because of the textured front surface and the planar rear surface. The tp-solar cell benefits from a rear reflector but it is unimportant which rear reflector. These results also confirm the optical results. The rear reflectors show a higher EQE enhancement for the tt-solar cell than for the tp-solar cell. This results from the higher transmission of the tt-solar cell [14].

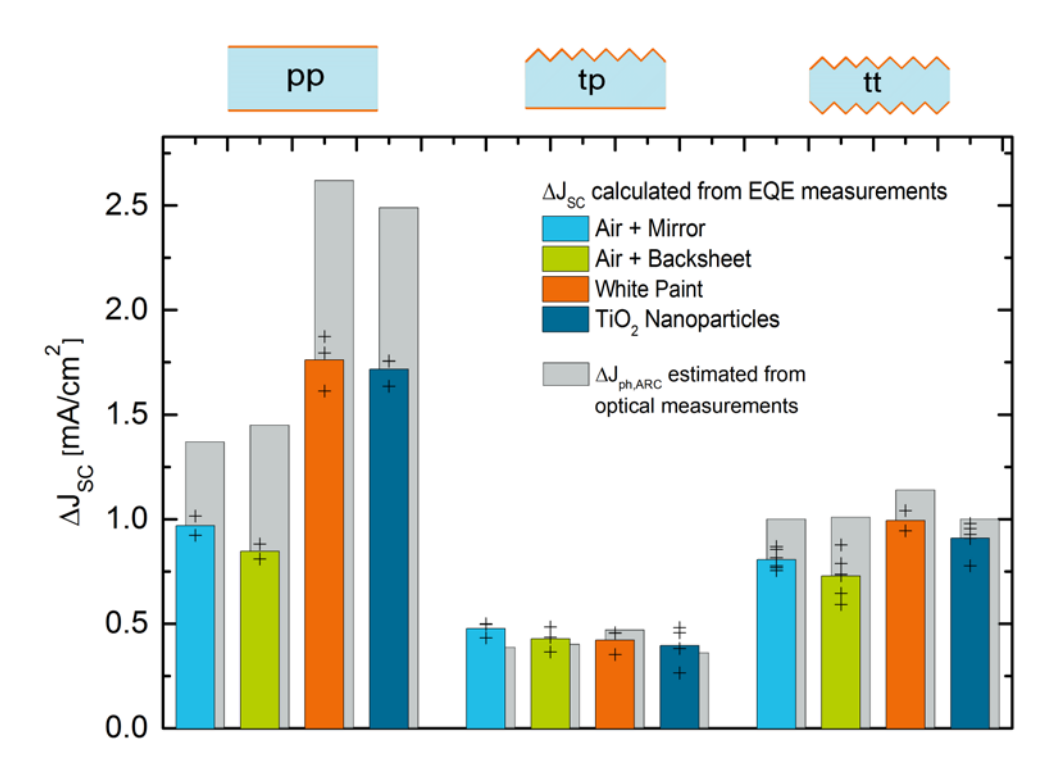


Figure 7: Photo current density gain (based on EQE-measurements) in comparison with a black reflector at the rear side. The J_{SC} and $J_{ph,ARC}$ were integrated between 900 and 1200 nm corresponding to equation 1. The colored bars represent the mean value of the electrical measurements. The gray bars represent the calculated photo-current gain with estimated ARC. The crosses indicate individually measured solar cells.

From the EQE data, we calculated the short-circuit current density gain ΔJ_{SC} between 900 and 1200 nm for the different rear reflectors in comparison to the black cardboard rear reflector. In Figure 7, the results obtained from one single measurement are displayed as a cross, to indicate the deviation between identically processed samples. The mean value is displayed as colored bar. The variations are caused by small differences between the solar cells, the coating processes and the measurement uncertainty. For a comparison of the optical and electrical results, the gray bars represent the gain $\Delta J_{ph,ARC}$ obtained from the optical measurements including the estimation of an ARC. There are different effects causing deviations between the optical and electrical measurements: first, comparing photo current densities with short circuit current densities assumes a carrier collection efficiency of 100 %. Our cells feature an IQE above 0.99 in the visible wavelength range, which indicates a very high collection efficiency. However, it might contribute to the overall deviation. Second, the (parasitic) absorption within the rear side reflector materials is included in the optically measured absorptance, and therefore contributes to a higher $\Delta J_{\mathrm{ph,ARC}}$ estimated from those measurements, but in fact does not contribute positively to the EQE. Additionally, the solar cells feature a front side grid leading to shadowing and a rear side grid slightly reducing the effective area of the reflector. With respect to these effects, the optical measurements can be understood as upper limits for the short circuit current density gain that could be reached. In summary, while the precise quantitative values predicted by optical measurements slightly differ from the final characterization with solar cells, the qualitative results of optical and electrical measurements are in good accordance to each other and we assess the absolute values determined with solar cells as our final results.

Table 2: $\Delta J_{\text{ph,ARC}}$ and integrated ΔJ_{SC} between 900 and 1200 nm. For integrated J_{SC} between 280 and 1200 nm, the mean value of the measurements is shown, corresponding to the colored bars in Figure 7. The gain was calculated in comparison to black cardboard as rear reflector for both the electrical and optical measurements. The values in brackets are the values reported by Frank et al. [14].

	planar/planar (pp)		texture/planar (tp)		texture/texture (tt)	
$J_{\rm SC}$ [mA/cm ²] 280 - 1200nm with black rear reflector	34.0		39.7		36.5	
Rear Reflector	$\Delta J_{ m ph}$ [m/	$\Delta J_{ m SC}$ A/cm²]	$\Delta J_{ m ph}$ [m/	$\Delta J_{ m SC}$ $\Delta/{ m cm^2}]$	$\Delta J_{ m ph}$ [m/	$\Delta J_{ m SC}$ A/cm ²]
Air + Mirror	1.4	1.0	0.4	0.5	1.0	0.8
Air + Backsheet	1.5	0.9	0.4	0.5	1.0	0.7
White Paint	2.6 (2.3)	1.8	0.5 (0.3)	0.4	1.1 (1.9)	1.0
TiO ₂ Nanoparticles	2.5	1.7	0.4	0.4	1.1	0.9

The current density gains are summarized in Table 2. One has to keep in mind that the solar cells have been originally designed for upconversion experiments and thus the absolute values J_{SC} are not optimized. We observed a gain ΔJ_{SC} for the pp-solar cells between 0.9 mA/cm² for the backsheet and over 1.7 mA/cm² for white paint and TiO₂ nanoparticles. Compared with the optical samples in Figure 5, the solar cell with white paint and TiO₂ nanoparticles show a 0.8 mA/cm² lower current gain. This is caused by the effects discussed above. The difference in the gain for the backsheet is smaller than for white paint and TiO₂ nanoparticles, although the backsheet has a higher parasitic absorption (see Figure 4); this is caused by the generally lower light trapping due to the air gap. The mirror shows similar results as the backsheet. For the tp-solar cells, the gain deduced from the electrical and optical measurements is very similar and lies within the variation of the individual measurements. For the tt-solar cells, a generally lower influence of parasitic absorption in comparison with the pp-solar cell, can be observed. This is caused by the textured surfaces and the generally better light trapping. White paint and TiO₂ nanoparticles show the highest current gain for the tt-solar cell (about 1 mA/cm²). The mirror and the backsheet show a similar gain of 0.7 and 0.8 mA/cm². The values in brackets are taken from [14]. Qualitatively, those values fit to the results obtained in this work. However, the gain observed for tt cells is significantly smaller than reported in [14].

To visualize the J_{SC} varying due to different rear side reflectors, we did a light beam induced current (LBIC) imaging for a $12.5 \times 12.5 \text{ cm}^2$ bifacial textured-textured solar cell. The result shows that the diffuse rear reflector systems, especially the deposition of TiO_2 nanoparticles, also work on large area solar cells. To each quarter of the solar cell we applied a different rear side reflector: white paint, TiO_2 nanoparticles, backsheet and black cardboard. Figure 8 shows that white paint and TiO_2 nanoparticles on the left side have a similar J_{SC} as expected from the EQE measurements. They show a higher J_{SC} enhancement than the backsheet, this also fits well to the optical end electrical results.

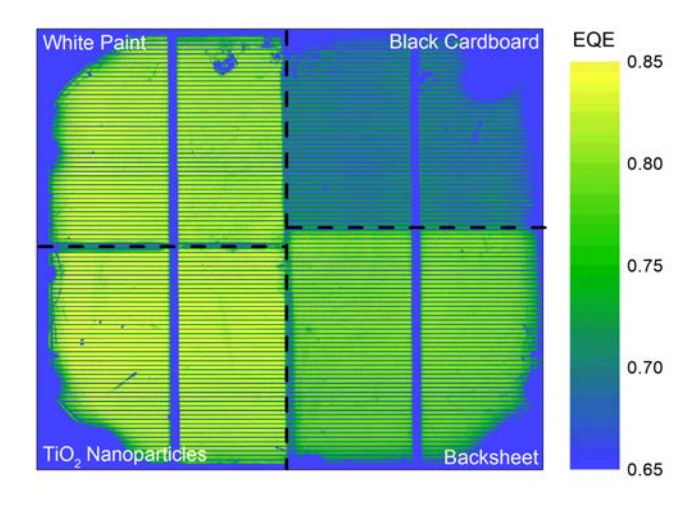


Figure 8: LBIC measurement of a 12.5×12.5 cm² bifacial solar cell at an excitation wavelength of 1064 nm. Behind each quarter we placed a different diffuse rear reflector. The white paint and TiO_2 nanoparticles, the backsheet and black cardboard were placed behind the bifacial solar cell starting in the left top corner clockwise. The EQE enhancements seen here fit to the optical and electrical results presented above.

In this work, we set a benchmark for simple diffuse light trapping structures for wafer based silicon solar cells. The quantitative results obtained here can now be compared to previously published studies mentioned in the introduction. For pp solar cells we found a current gain of less than 1 mA/cm² due to simple diffuse rear reflectors in comparison to a mirror at the rear side. This value is smaller than the values cited in the introduction for the pp solar cells with more complex rear side structures based on diffractive gratings (1.5, 1.2 and 1.4 mA/cm² based on [21,25,26]). Nonetheless, roughly half of that gain is reached with the very simple reflectors presented here. Considering the results of other concepts in the field of thin film silicon photovoltaics cited in the introduction, a direct quantitative comparison is difficult. For thick solar cells like in this work only the redirection of light due to a reflector has to be considered, whereas in thin film solar cells near field effects and coherent coupling of front and rear play an important role. Of course, the current gain values stated in this work for 200 µm thick cells would increase for thinner silicon wafers or thin films. The statement of Frank et al. [14] that tt cells with a good rear side reflector show the overall highest photo current density cannot be confirmed in experiment here. The tt solar cells feature a higher current gain than the tp solar cells; however, this cannot compensate for their originally significantly lower current. This is likely also related to details in the processing of the tt cells, which could have a lower current due to factors other than optical effects (for example poorer rear side passivation for the textured cells). Thus, we cannot make a firm conclusion about which system is the best overall, within this work.

4. Conclusion

In this study, we systematically analyzed different simple diffuse rear reflectors for the enhancement of light trapping in silicon solar cells. We investigated white paints, commercial backsheets and TiO₂ nanoparticles. For reference we also investigated a highly reflective silver mirror and black cardboard. We performed optical measurements on planar wafers (pp) and wafers with random pyramids either only on the front side (tp) or on both sides (tt). By reflectance and transmittance measurements an absorption enhancement was determined for all reflectors. White paint as well as TiO₂ nanoparticles showed the highest absorption enhancements. We also compared the different reflectors on fully processed solar cells. For all reflectors, we measured the external quantum efficiency of originally bifacial solar cells with an active area of 2x2 cm². The solar cells we used featured three different combinations of surface morphologies:

planar front and rear surface (pp), textured front surface with inverted pyramids and planar rear surface (tp), and both sides textured with inverted pyramids (tt). The electrical measurements confirmed the optical measurements. For pp solar cells, white paint and TiO_2 nanoparticles lead to an enhancement of more than 1.7 mA/cm² in comparison to gain values below 1 mA/cm² for a silver mirror or for a backsheet. This leads to an overall J_{SC} of up to 36 mA/cm² for the used solar cells featuring non-optimized antireflection coatings. For tp and tt solar cells all reflector types showed a similar J_{SC} gain, because the structuring of the solar cell already enhances the path length of near infrared photons. In addition to the EQE-analysis we did a light beam induced current (LBIC) measurement on a solar cell with an active area of $12.5 \times 12.5 \text{ cm}^2$. The LBIC measurement demonstrates the locally varying short circuit current density gain depending on the rear reflector type and also demonstrates the applicability of all used rear reflectors to large area solar cells. The attained values can be seen as a useful benchmark for more complex and expensive light trapping structures, which are capable of achieving up to twice the absorption enhancement as our best investigated diffuse reflectors on wafers of comparable thickness.

Acknowledgements

The authors would like to thank A. Leimenstoll, F. Schätzle, S. Seitz, N. Weber, K. Zimmermann, C. Follert and especially E. Schäffer for their support with processing and measurements. This work was partially funded by the German Federal Ministry for Economic Affairs and Energy under contract number 0325292 (ForTeS). J. Eisenlohr gratefully acknowledges scholarship support from the Deutsche Bundesstiftung Umwelt DBU.

References

- [1] P. Campbell, M.A. Green, Light trapping properties of pyramidally textured surfaces, J Appl Phys 62 (1987) 243–249.
- [2] P. Campbell, S.R. Wenham, M.A. Green, Light trapping and reflection control in solar cells using tilted crystallographic surface textures, Sol Energ Mat Sol C 31 (1993) 133–153.
- [3] P. Campbell, Light trapping in textured solar cells, Solar Energy Materials 21 (1990) 165–172.
- [4] D. Kray, M. Hermle, S.W. Glunz, Theory and experiments on the back side reflectance of silicon wafer solar cells, Prog. Photovolt: Res. Appl. 16 (2008) 1–15.
- [5] A. Goetzberger, Optical confinement in thin Si-solar cells by diffuse back reflectors, in: Proceedings of the 15th IEEE Photovoltaic Specialists Conference, 1981, pp. 867–870.
- [6] E. Yablonovitch, Statistical ray optics, J. Opt. Soc. Am. 72 (1982) 899–907.
- [7] J.E. Cotter, Optical intensity of light in layers of silicon with rear diffuse reflectors, J. Appl. Phys. 84 (1998) 618.
- [8] O. Berger, D. Inns, A.G. Aberle, Commercial white paint as back surface reflector for thin-film solar cells, solar Energy Materials and Solar Cells 91 (2007) 1215–1221.
- [9] C. Barugkin, T. Allen, T.K. Chong, T.P. White, K.J. Weber, K.R. Catchpole, Light trapping efficiency comparison of Si solar cell textures using spectral photoluminescence, Opt. Express 23 (2015) A391.
- [10] A. Basch, F. Beck, T. Söderström, S. Varlamov, K.R. Catchpole, Enhanced light trapping in solar cells using snow globe coating, Prog. Photovolt: Res. Appl. 20 (2012) 837–842.
- [11] B.G. Lee, P. Stradins, D.L. Young, K. Alberi, T.-K. Chuang, J.G. Couillard, H.M. Branz, Light trapping by a dielectric nanoparticle back reflector in film silicon solar cells, Appl. Phys. Lett. 99 (2011) 64101.

- [12] A. Ingenito, S.L. Luxembourg, P. Spinelli, J. Liu, J.C. Ortiz Lizcano, A.W. Weeber, O. Isabella, M. Zeman, Optimized Metal-Free Back Reflectors for High-Efficiency Open Rear c-Si Solar Cells, IEEE J. Photovoltaics 6 (2016) 34–40.
- [13] B. Bills, N. Morris, M. Dubey, Q. Wang, Q.H. Fan, Electrophoretic deposited TiO_2 pigment-based back reflectors for thin film solar cells, Opt. Express 23 (2015) A71.
- [14] J. Frank, M. Rüdiger, S. Fischer, J.C. Goldschmidt, M. Hermle, Optical Simulation of Bifacial Solar Cells, Energy Procedia 27 (2012) 300–305.
- [15] C. Heine, R.H. Morf, Submicrometer gratings for solar energy applications, Appl. Opt. 34 (1995) 2476–2482.
- [16] P. Bermel, C. Luo, L. Zeng, L.C. Kimerling, J.D. Joannopoulos, Improving thin-film crystalline silicon solar cell efficiencies with photonic crystals, Opt. Express 15 (2007) 16986–17000.
- [17] Z. Yu, A. Raman, S. Fan, Fundamental limit of light trapping in grating structures, Opt Express 18 (2010) A366-A380.
- [18] M. Peters, M. Rüdiger, H. Hauser, M. Hermle, B. Bläsi, Diffractive gratings for crystalline silicon solar cells—optimum parameters and loss mechanisms, Prog Photovoltaics 20 (2012) 862–873.
- [19] A. Mellor, H. Hauser, C. Wellens, J. Benick, J. Eisenlohr, M. Peters, A. Guttowski, I. Tobias, A. Marti, A. Luque, B. Bläsi, Nanoimprinted diffraction gratings for crystalline silicon solar cells: implementation, characterization and simulation, Opt Express 21 (2013) A295-A304.
- [20] J. Eisenlohr, J. Benick, M. Peters, B. Bläsi, J.C. Goldschmidt, M. Hermle, Hexagonal sphere gratings for enhanced light trapping in crystalline silicon solar cells, Opt. Express 22 (2014) A111-A119.
- [21] J. Eisenlohr, B.G. Lee, J. Benick, F. Feldmann, M. Drießen, N. Milenkovic, B. Bläsi, J.C. Goldschmidt, M. Hermle, Rear side sphere gratings for improved light trapping in crystalline silicon single junction and silicon-based tandem solar cells, Solar Energy Materials & Solar Cells 142 (2015) 60–65.
- [22] K.R. Catchpole, S. Mokkapati, F. Beck, E.C. Wang, A. McKinley, A. Basch, J. Lee, Plasmonics and nanophotonics for photovoltaics, Mrs Bull 36 (2011) 461–467.
- [23] F.J. Beck, S. Mokkapati, K.R. Catchpole, Light trapping with plasmonic particles: beyond the dipole model, Opt Express 19 (2011) 25230–25241.
- [24] A. Ingenito, O. Isabella, M. Zeman, Experimental demonstration of 4 n2 classical absorption limit in nanotextured ultrathin solar cells with dielectric omnidirectional back reflector, ACS Photonics 1 (2014) 270– 278.
- [25] A. Mellor, H. Hauser, C. Wellens, J. Benick, J. Eisenlohr, M. Peters, A. Guttowski, I. Tobías, A. Martí, A. Luque, B. Bläsi, Nanoimprinted diffraction gratings for crystalline silicon solar cells: implementation, characterization and simulation, Opt Express 21 Suppl 2 (2013) A295-304.
- [26] N. Tucher, J. Eisenlohr, H. Hauser, J. Benick, M. Graf, C. Müller, M. Hermle, J.C. Goldschmidt, B. Bläsi, Crystalline silicon solar cells with enhanced light trapping via rear side diffraction grating, Energy Procedia 77 (2015) 253–262.
- [27] S.W. Glunz, High-efficiency crystalline silicon solar cells, Advances in OptoElectronics 2007 (2007) 97370.
- [28] M. Rüdiger, S. Fischer, J. Frank, A. Ivaturi, B.S. Richards, K.W. Krämer, M. Hermle, J.C. Goldschmidt, Bifacial n-type silicon solar cells for upconversion applications, Solar Energy Materials & Solar Cells 128 (2014) 57–68.
- [29] IEC, Photovoltaic devices part 3: measurement principles for terrestrial photovoltaic (PV) solar devices with reference spectral irradiance data., 2nd ed., International Electrotechnical Commission, 2008.

